Offshore anchor piles under mooring forces: centrifuge modeling

Mohamed I. Ramadan, Stephen D. Butt, and R. Popescu

Abstract: Offshore anchor piles are seafloor moorings that keep the position of floating structures during a harsh environment. These piles are usually subjected to a wide range of monotonic and cyclic lateral-to-oblique pullout forces. Centrifuge tests were carried out to study the behavior of offshore anchor piles under mooring forces in saturated dense sand. The tests were carried out at different loading angles. All piles were jacked into the sand bed in-flight. The pile models were instrumented with strain gauges. Bending moment, soil pressure, and pile lateral deflection profiles are presented and discussed. It was found that there is a significant interaction between both tension and lateral loading. This interaction should be considered in the design of offshore anchor piles.

Key words: offshore, anchor pile, dense sand, centrifuge, inclined loading.

Résumé : Les pieux d'ancrage en mer sont des corps d'amarrage sur le fond marin qui maintiennent la position des structures flottantes durant les conditions environnementales difficiles. Ces pieux sont généralement soumis à une variété de forces de retrait latérales monotoniques et cycliques et même obliques. Des essais par centrifugeuse ont été réalisés pour étudier le comportement de pieux d'ancrage en mer soumis à des forces d'amarrage dans du sable dense saturé. Les essais ont été effectués à différents angles de chargement. Tous les pieux ont été placés dans le sable en vol par un vérin. Les modèles de pieux ont été instrumentés avec des jauges de déformation. Cet article présente et discute les moments de torsion, la pression du sol et les profils de déflection latérale des pieux. Il a été déterminé qu'il existe une interaction significative entre la tension et le chargement latéral. Cette interaction devrait être prise en compte lors de la conception de pieux d'ancrage en mer. [Traduit par la Rédaction]

Mots-clés : en mer, pieu d'ancrage, sable dense, centrifugeuse, chargement incline.

Introduction

Floating production storage offloading vessels (FPSOs) are widely used in the offshore oil and gas industry in harsh environments at the Grand Banks, east of Newfoundland, Canada. Vessels working at an offshore site must be held in position despite the effects of wind, waves, and current. Many FPSOs are keeping position using seafloor, anchors which are commonly secured using anchor piles, as shown in Fig. 1. Anchor piles are very effective in many soils. The anchor pile resists pullout by a combination of bending plus passive resistance and skin friction shear. Also, a careful location of the pad eye along the pile length can control the anchor pile pullout resistance.

There is relatively limited experimental information on anchor piles or piles subjected to oblique pull loads. Due to the great complexity of the response mechanism of an obliquely loaded anchor pile, this problem has received very little attention. The analyses proposed have made very crude assumptions that may invalidate their applicability to full scale. Most of the research done in this area was for lateral or tension loads on the piles. The effect of horizontal and vertical components of applied load has been assumed to be uncoupled (Hesar 1991). Bhattacharya et al. (2006) reported that the geotechnical analysis of an FPSO pile can be de-coupled, in the sense that the axial and lateral capacities can be considered independently. Their assumption is considered valid based on the understanding that the axial tension capacity is provided by the soil around the lower part of the pile, whereas lateral resistance is provided mainly by the soil around the upper part of the pile, typically to a depth of 3 to 6 times the diameter of

the pile. In addition, the lateral load component loads the soil passively whereas the axial tension load component loads the soil in shear. Therefore, they suggested no significant interaction is expected for long piles. However, for short piles both lateral and axial pullout load components will interact. It should be noted that the assumption of de-coupling of lateral and axial pullout components for long piles may not be valid for offshore driven pipe piles as will be discussed in the present paper.

Some of the existing theoretical models are semi-empirical based on 1g experimental tests, such as Yoshimi (1964), Broms (1965), Das et al. (1976), Chattopadhyay and Pise (1986), and Jamnejad and Hesar (1995). As indicated by Altaee and Fellenius (1994), the dilation of the sand occurring at low confining stress – shallow depth increases the lateral soil pressure against the pile. This means that 1g test results cannot be extrapolated to the prototype scale if physical modeling scaling laws are not considered. Even field tests carried out by Leshukov (1975) and Ismael (1989) using small-scale piles will only eliminate the boundary conditions problem in the laboratory test. However, the physical modeling scaling laws will not be controlled and therefore their results cannot correctly reproduce the real behavior of the prototype-scale piles in sandy soil. In addition, with the exception of Chattopadhyay and Pise (1986) and Jamnejad and Hesar (1995), no account has been taken of the flexibility of the anchor pile. Other models are based on the net uplift and the ultimate lateral capacity of the pile, whichever is smaller, as reported by Poulos and Davis (1980), and neglected the interaction between horizontal and vertical pull forces on the pile. Abdel-Rahman and Achmus (2006) and Achmus et al. (2007) did a finite element (FE) analysis to
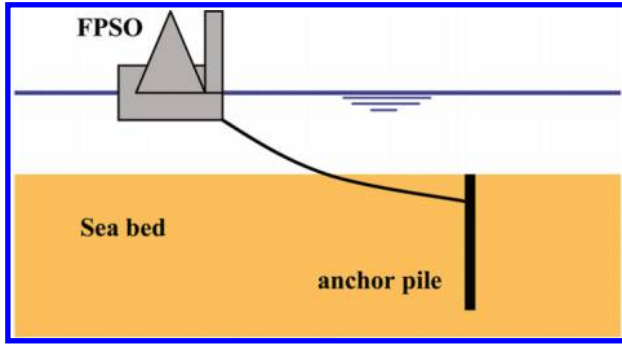
M.I. Ramadan. Civil Engineering Department, Assiut University, Assiut, Egypt.
S.D. Butt. Faculty of Engineering, Memorial University of Newfoundland, St. John's, NL, Canada.
R. Popescu. URS Corporation, Princeton, NJ, USA.

Corresponding author: Mohamed I. Ramadan (e-mail: mohamedihr@mun.ca).

Fig. 1. Schematic diagram of FPSO and anchor pile.

study the interaction between horizontal and vertical pullout loads for offshore piles. They suggested that this interaction must be considered in the determination of axial displacements under tension loading and thus in the serviceability design. Although the horizontal capacity is little affected by the tension capacity under monotonic loads, it is necessary to check against the tension failure, as skin friction will be reduced in the upper part of the pile due to the gap formation surrounding the pile during repeated cyclic loading.

From the previous discussion, it can be seen that there is a need to do experimental research to study the behavior of this interaction under monotonic and cyclic loads. Ramadan et al. (2009a) carried out a numerical study using three-dimensional (3D) FE to study the behavior of offshore anchor piles in dense sand under mooring forces. They found that the ultimate resistance of a pile under oblique pull is a continuous function of the inclination of the pull and depends also on the net uplift and the ultimate lateral capacity of the pile. Comparing their results with the previous theoretical models shows that most of the available models did not consider the prototype scale. So, they should be modified to be practically useful. However, in their study, the effect of pile installation was not considered. Ramadan et al. (2009b) carried out the same study as Ramadan et al. (2009a), considering the effect of pile installation. It was observed that the oblique ultimate capacity is highly influenced by the tension load component. Even for a small inclination angle of 15° to horizontal, the ultimate capacity is higher than that for pure lateral loading.

The presented research aims at identifying the behavior and capacity of anchor piles used for anchoring offshore floating structures in dense sand. As full-scale experimental verification is not always possible, this raises the need to design a physical model that can simulate the behavior of full-scale case. To simulate the important gravitational component, the physical model tests were conducted using a geotechnical centrifuge to investigate the anchor piles response to mooring forces in saturated dense sand. A series of centrifuge tests was carried out at C-CORE, Memorial University of Newfoundland. The main objective of these tests is to understand the interaction between the lateral and vertical pullout response of the piles under combined loads. The experimental results will be used (in a companion paper) to calibrate a 3D finite element model (FEM) that can be used in a parametric study to provide design methods for offshore anchor piles under mooring forces.

Experimental program and setup

Centrifuge modeling has been used extensively over the previous decades in geotechnical engineering. It has the capability to achieve stress similarity between model and prototype. Such similarity cannot be achieved at 1g model tests, especially for deep depth models as piles.

Six centrifuge tests were undertaken to investigate the behavior of offshore anchor piles under mooring forces. Five tests were loaded monotonically at 70g and the other test was loaded monotonically at 50g. All tests were carried out under drained conditions.

Soil properties

Fraser River sand was used in the experiment. It has been selected because of its availability at C-Core, it has been extensively used in centrifuge testing, and its properties are well known. As reported by Wijewickreme et al. (2005), theFraser River sand that was used in the present tests has an average particle size, d_{50} (at which 50% of the mass of a soil specimen is finer) = 0.26 mm; soil particle diameter d_{10} (at which 10% of the mass of a soil specimen is finer) = 0.17 mm; specific gravity, G_s = 2.71; and uniformity coefficient, C_u = 1.6. The maximum and minimum void ratios (e_{max} and e_{min}) for the sand are 0.94 and 0.62, respectively. The sand grains are generally angular to subrounded. In the case of piles in sand, the size of soil particles relative to pile diameter may have a significant effect. Ovesen (1979) showed that the scale effects are negligible on shallow foundation bearing capacity studies if the ratio D/d_{50} is larger than 30, where D is the foundation depth. Remaud (1999) performed a series of "modeling of models" tests on the same pile under lateral loads. No scale effects were observed for $d/d_{50} > 60$, where d is pile diameter. In the present study, the d/d_{50} ratio is about 77.
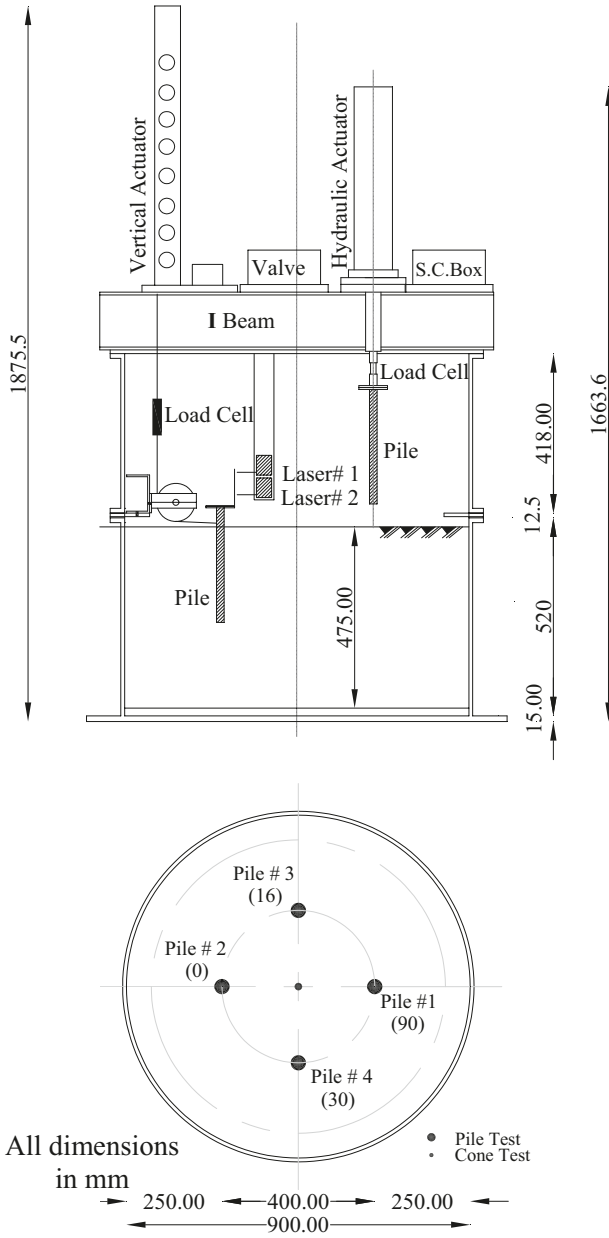
Soil container and sample preparation

All tests were carried out in a round steel tub of 914 mm diameter and 500 mm height, as shown in Fig. 2. The sand was prepared by dry air pluviation into the model container using a hopper. The characteristic variation of Fraser River sand relative density with average fall height determined by Chakrabortty (2008) was used in the present test preparation. During model preparation the hopper was kept at a constant speed of about 10 cm/s and a constant height of 1.2 m to the tub base. Three density cups were used to check the relative density of the rained sand at the bottom, middle, and top of the soil model. The average relative density was 86%. After raining the sand into the tub up to a height of 470 mm, the tub was sealed at the top and the saturation process was started using de-aired water as described by Dief (2000). Two in-flight cone penetration tests (CPTs) were performed at 50g and 70g to check the repeatability of the sand models as shown in Fig. 3. The results of the CPTs were used to calculate the angle of internal friction.

Model pile

Instrumented open-ended model piles were made of aluminum. The dimensions of the model piles were 18 mm by 1.5 mm by 300 mm in outside diameter, wall thickness, and pile length, respectively, as shown in Fig. 4. The embedment depth of the pile was 250 mm, which gives a length to diameter ratio (L/d) of 12.5. For FPSO piles, Bhattacharya et al. (2006) reported that pile length usually ranges between 15 and 25 m. They also reported that pile diameter ranges between 1 and 2 m. FPSO piles at offshore Newfoundland sites have pile diameters of 2 m and pile lengths of 30 m, which gives an L/d value of 15. Based on these dimensions and the test boundary effects, and due to pile jacking problems at high g-levels, and L/d ratio of 12.5 was selected.

All model piles were instrumented with 10 pairs of strain gauges. The model pile had been coated with a thin layer of 1 mm of epoxy resin. This layer protected the strain gauges on the pile surface from being damaged during pile jacking into the sand and by water. This protective layer increased the diameter of the pile to 20 mm without modifying the pile stiffness as found from the calibration tests. From these strain gauges the bending moment profile at 10 levels in addition to the calculated bending moment at the ground surface (total of 11 levels) versus depth was achieved. The prototype pile properties are shown in Table 1. The epoxy layer provided a smooth surface for the pile surface. De Nicola and Randolph (1999) recommended a value of 0.53 for the friction

Fig. 2. Test setup and location of the piles and cone tests.

All dimensions
in mm

250.00 400.00 250.00
900.00

Fig. 3. Cone penetration tests at 70g and 50g.

a pad eye 10 mm above the sand surface. The loading angle was controlled by passing the loading cable over a ball bearing pulley. The pulley level can be changed at different levels to get the required loading angle to horizontal at the pad eye. This load was measured with an in-line load cell of 2.5 kN capacity. The measured load was the total inclined pullout load at the pile head. The loading rate was constant throughout all tests, at a displacement-controlled rate of 0.10 mm/s to satisfy drained conditions as suggested by Nunez et al. (1988) and Dyson and Randolph (2001). The loading device details are shown in Fig. 2.

Due to cable stretching during loading, the controlled displacement was not the displacement at the pile head. Therefore, two laser displacement transducers mounted at different levels above the pile head were used to measure the actual pile head displacements, as shown in Fig. 2. The measured displacements allowed estimation of pile head rotation and lateral displacement.

Loading test program

Five piles were tested at 70g. These piles were loaded at loading angles (θ) of 0°, 3°, 16°, 30°, and 90° to horizontal. Another pile was tested at 50g and loaded at θ = 90° to horizontal (pure tension loading). For piles tests loaded at 3°, only the load at the pile head and bending moment profile were obtained. In the following sections the analysis of the results will be discussed.

Test results and analysis

Load–displacement curves were obtained from all tests. For piles that had been tested under lateral loading, bending moment profiles were obtained. The measured bending moment was fitted by a quintic spline function and then differentiated twice to get the soil pressure (P) and integrated twice to get the pile deflection (y). At some load increments p–y curves can be derived at different depths. All results will be presented at prototype scale.

Tension loading

Figures 5 and 6 show the vertical load (V) – normalized vertical displacement (v/d) curves for tension tests at 70g and 50g, respectively. In the case of the 70g test, the pile was installed in-flight by jacking and then pulled out with the same hydraulic actuator without stopping the centrifuge in between the two processes. In the case of the 50g test, the centrifuge was stopped after pile installation and then the pile was pulled out in another flight. The ultimate tension capacity of both centrifuge tests can be compared to that calculated using the Imperial College pile (ICP) method (Jardine et al. 2005). For the centrifuge test at 70g, the ultimate tension capacity is about 33 MN. However, the ultimate tension capacity calculated using the ICP method is about 7 MN, with a difference about 80% lower than the centrifuge test. For the centrifuge test at 50g, the ultimate tension capacity is about 2.5 MN. However, the one calculated using the ICP method is about 2.1 MN, with a difference 16% lower than the centrifuge test. Figure 7 shows the measured axial load along the pile at the strain gauge locations for the 70g test. The distribution of axial load

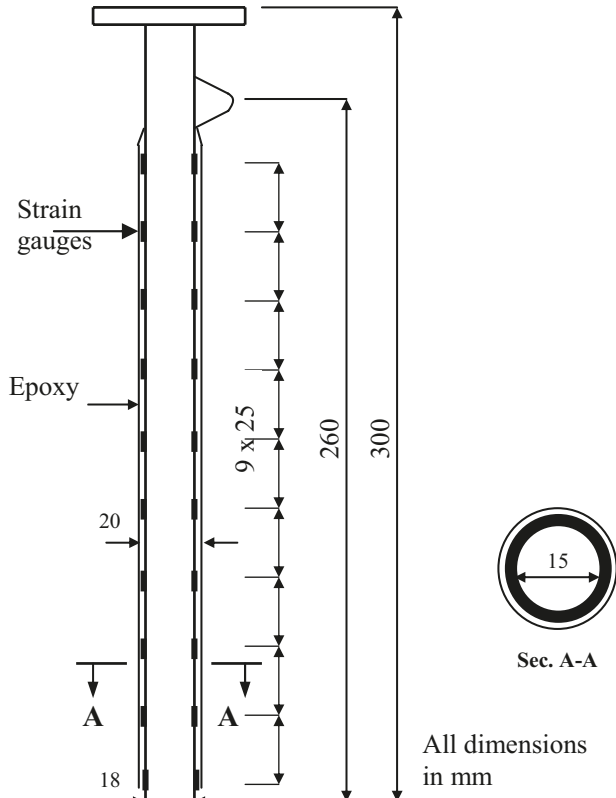coefficient between epoxy surface and sand in their centrifuge tests.

Pile installation

The model piles were kept hanging, attached to the hydraulic actuator in air before spinning up the centrifuge as shown in Fig. 2. After spinning up the centrifuge, the pile was jacked into the sand bed. All piles were fully installed in-flight into the sand bed at the same g-level of the loading tests. The jacking rate was 0.1 mm/s to ensure drained conditions as recommended by Dyson and Randolph (2001). Once the pile had penetrated 250 mm (17.5 and 12.5 m at 70g and 50g in prototype dimensions, respectively) into sand bed, the hydraulic actuator was stopped and the centrifuge was stopped to disconnect the hydraulic actuator from the pile. Then the bottom tub was rotated to hook up the pile to the loading device.

Loading device

The load was transferred to the pile through a stainless steel flexible aircraft cable. The cable was connected to the pile through

Fig. 4. Instrumented pile.

Strain gauges

Epoxy

9 x 25

260

300

20

15

Sec. A-A

A   A

18

All dimensions in mm

Table 1. Prototype pile characteristic at 70g and 50g tests.

	Prototype	
Characteristic	70g	50g
Length up to loading point (m)	18.2	13
Embedded length (m)	17.5	12.5
External diameter (m)	1.4	1.0
Young's modulus, E (MPa)	2.1×10^5	2.1×10^5
Flexural stiffness (MPa)	4484.0	1167.23

Fig. 5. Vertical load versus normalized vertical displacement at pile head – 70g test.

Fig. 6. Vertical load versus normalized vertical displacement at pile head – 50g test.
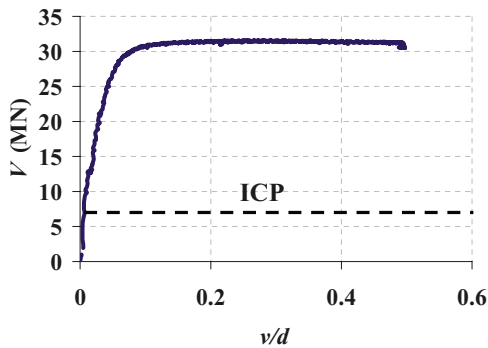
shows compression residual load after pile installation. After installation, the pile was kept connected to the hydraulic jack. The tension test was started 5 min after pile installation to allow for stress relaxation around the pile. Once tension loading started, a sudden increase of about 10 MN at the pile tip was observed, as shown in Fig. 7. In the literature, most centrifuge tests carried out on open-ended piles in dense sand were done by driving the pile using a hammer before loading in tension. In driven piles cases, after each blow the pile loses part of the energy transferred to it from the hammer by moving up a little. Such a movement will allow the residual load at pile tip to decrease. In other tests, the open-ended pile was jacked into dense sand and then loaded in compression before tension loading. It should be noted that the tendency of driven open-ended piles to plug is less than that for jacked open-ended piles, as discussed by De Nicola and Randolph (1997). In our centrifuge tests, soil plug height was about 30% of pile embedded length. At the pile tip, both the bearing resistance of dense sand and the dilation effect will cause high normal stresses between the soil plug and the pile (De Nicola and Randolph 1997). The effect of dilation is magnified for small-scale model piles than for large piles. In the ICP method, the stress change due to dilation effects during tension loading ($\Delta\sigma'_{rd}$) is considered (where $\Delta\sigma'_{rd} = 4GR_{calc}/d$, with G being the soil shear modulus and R_{calc} the pile surface roughness). Jardine et al. (2005) reported that the change in radial effective stress during pile loading may contribute less than 5% of the capacity for piles with diameters greater than 1 m. However, this dilation term is important with medium-scale piles and can dominate the behavior of small model piles because of the inverse dependence of $\Delta\sigma'_{rd}$ on the diameter. For the 50g test, the centrifuge was stopped in between the processes of jacking and tension loading. The centrifuge stopping effect can be seen in the reduction of shear stresses along the pile shaft as shown in Fig. 8. What can be concluded from this discussion is that the effect of dilation and soil plug interaction with pile caused high residual loads close to pile tip and a high overprediction of pile tension capacity (80% higher than that from ICP). However, in the case of the 50g test, stopping the centrifuge released the high stresses in the soil plug and the predicted tension capacity was only affected with the dilation effect due to the use of a small-scale pile (only 16% higher than ICP). In all the next lateral and inclined loading tests, the centrifuge was stopped to switch between the actuators. From the previous discussion it can be noted that stopping the centrifuge in our tests eliminated the overprediction in residual stresses around the pile.

Lateral loading

Load–displacement curves

Figure 9 shows the horizontal load (H) versus horizontal displacement at pile head (u) curves. It can be seen from the figures that as the loading angle (θ) increases from 0° (pure lateral loading) to 30°, the soil–pile system response (the load–displacement curve) becomes stiffer. At a pile head displacement of 10% of pile diameter, the carried load at the pile head increased 16.3% and 41.6% when θ increased to 16° and 30°, respectively.

Fig. 7. Axial load distribution along pile shaft – 70*g* test. *h*, distance measured from pile tip.

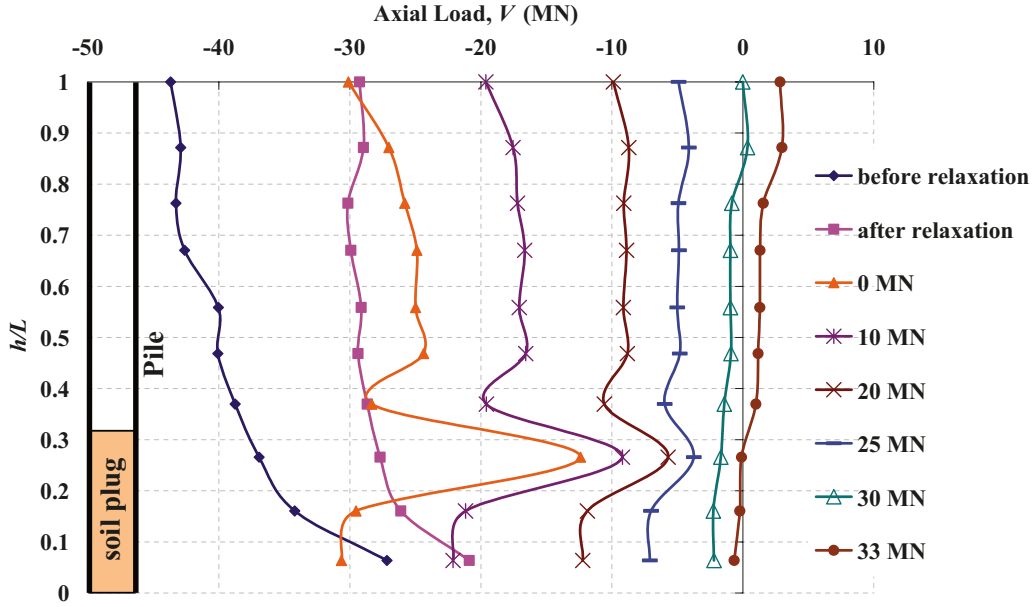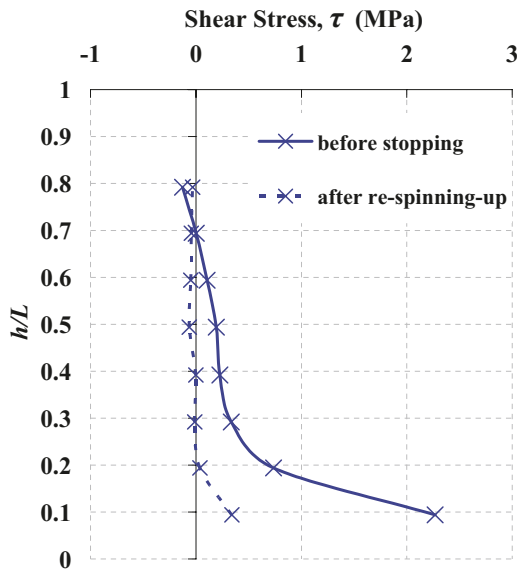**Fig. 8.** Shear stresses along pile shaft before spinning down and after re-spinning up – 70*g* test.

Fig. 9. Horizontal load versus horizontal displacement at pile head – 70*g* test.
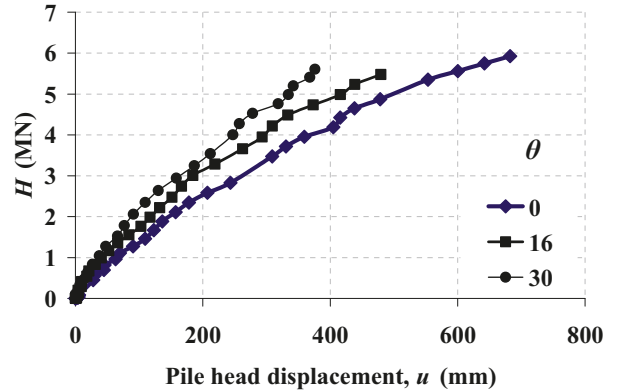

Bending moment curves

Figure 10*a* shows the discrete measured bending moment at the successful strain gauges for $\theta = 0°$ (pure lateral loading). A comparison between bending moment profiles of different θ values at horizontal load at a pile head (*H*) of 1500 kN is shown in Fig. 11*a*. The maximum bending moment values of all θ values larger than 0° at the same horizontal load increment are very close.

The relations between the normalized horizontal load (H_n) on the pile head and the normalized maximum bending moment ($M_{n\text{-max}}$) for all piles are shown in Fig. 12. Both H_n and $M_{n\text{-max}}$ can be defined as follows:

$$[1] \qquad H_n = \frac{H}{\gamma' d^3}$$

$$[2] \qquad M_{n\text{-max}} = \frac{M_{max}}{\gamma' d^4}$$

where M_{max} is the maximum bending moment and γ' is the effective unit weight of sand.

All data show a linear increase of $M_{n\text{-max}}$ as H_n increases. It can be seen that all piles tested at angles larger than 0° have almost the same ratio $M_{n\text{-max}}/H_n$, smaller than that for the pure lateral loading case. The data can be fitted to the following equation:

$$[3a] \qquad M_{n\text{-max}} = 2.47 H_n \quad \text{(pure lateral loading)}$$

$$[3b] \qquad M_{n\text{-max}} = 1.57 H_n \quad \text{(inclined pullout loading)}$$

This reduction is almost constant regardless of θ values. This means that the reduction is due to a reduction in soil confining pressure around the pile. The tension load component of the pullout force at the pile head causes elastic "Poisson" radial contractions of the shaft, which is more significant with tubular pile as reported by Jardine et al. (2005). This radial contraction of the pile section will cause a reduction in soil confining pressure around the pile and consequently a reduction in bending moment profile.

p–y curves

The experimental bending moment data were fitted using a quintic spline function. The fitted function was integrated twice

Fig. 10. Pure lateral loading case: (*a*) bending moment (the solid line is the fitting curve), (*b*) soil pressure, and (*c*) pile lateral deflection profiles – 70*g* test.
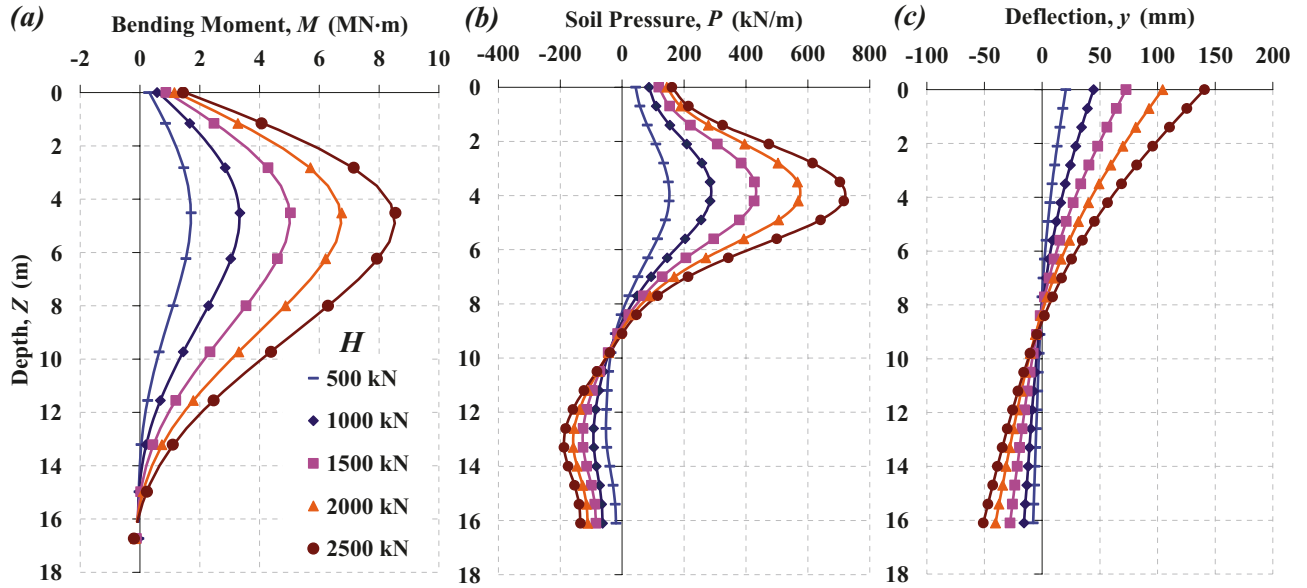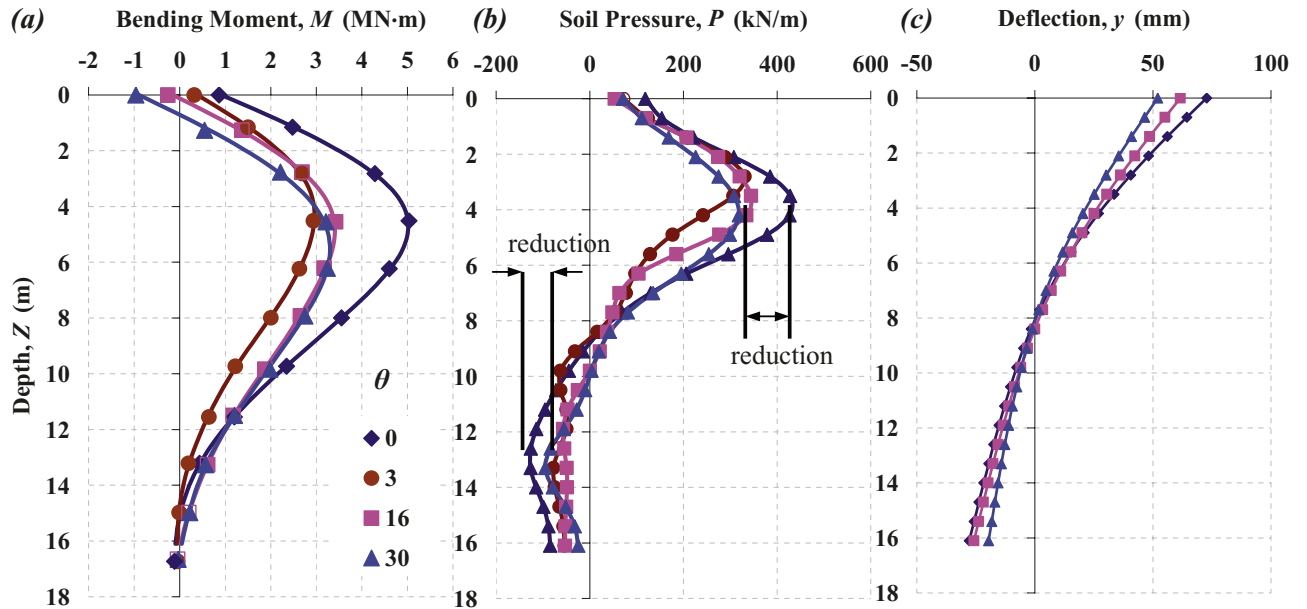

Fig. 11. Pile profiles different loading angles at *H* = 1500 kN: (*a*) bending moment (the solid line is the fitting curve), (*b*) soil pressure, and (*c*) pile lateral deflection profiles – 70*g* test.

to get the pile curvature and displacement profile (*y*). In the present study, the integration constants were the rotation and horizontal displacement from the two laser displacement transducers at the pile head. The fitted function was also differentiated twice to get the shear and soil pressure (*P*), in kN/m, along the pile length.

Quintic spline functions were found to provide the best fit of the experimental bending moment data and gave a smooth and an acceptable continuous profile for the soil pressure (*P*) and displacement (*y*) along the pile. As recommended by many authors (Mezazigh and Levacher 1998; Bouafia 1999), the fitting process was carried out using an adjustable smoothing parameter, ρ. The value of this parameter controls the smoothness of the fitted bending moment profile. The value of ρ is selected by checking the static equilibrium of the pile. Once the soil pressure (*P*) and the

displacement (*y*) profiles are obtained at different load increments at the pile head, *p*–*y* curves can be derived for all tests under lateral loading. The pressure curves *P(z)* are determined by double differentiation of the bending moment curves as

[4] $\qquad P(z) = \dfrac{\mathrm{d}^2 M(z)}{\mathrm{d}z^2}$

The pile deflection profiles, *y(z)*, have been determined by double integration of the bending moment curves as

[5] $\qquad y(z) = \dfrac{1}{E_p I_p} \int \int M(z)\,\mathrm{d}z^2$

Fig. 12. Normalized horizontal load versus normalized maximum bending moment.
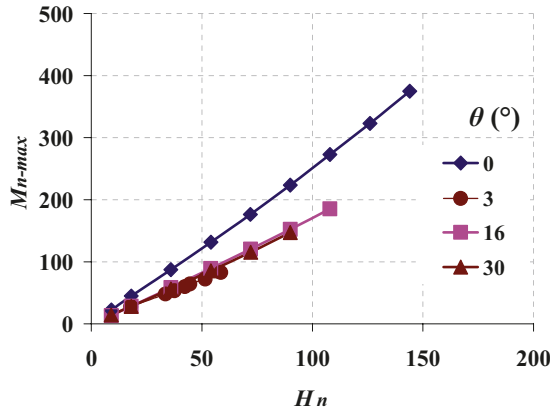
where E_p is the Young's modulus of the pile and I_p is the moment of inertia of the pile cross section.

Figure 10b show the soil pressure (P), in kN/m, profile versus depth (Z), in m, for the piles tested at $\theta = 0°$ at different load increments. A comparison between P profiles at different θ at a load increment (H) of 1500 kN is shown in Fig. 11b. It can be seen that P profiles are almost the same for loading angles larger than 0°. There is a significant reduction in maximum and minimum soil pressure values once θ changes from pure lateral loading to inclined pullout loading.

The pile lateral deflection (u) profile for the pure lateral loading and a comparison with different θ values are shown in Figs. 10c and 11c, respectively. It can be seen that pile rotation decreases by increasing θ. This trend is expected as the vertical pullout load component causes this decrease in the pile rotation.

For each depth, p–y curves have been plotted as shown in Fig. 13. When comparing these curves for different θ values at the same Z/d ratio, as shown in Fig. 14, it can be seen that the initial stiffness of the p–y curves is the same. It can be seen also that all p–y curves are nonlinear. All curves are of a parabolic shape with no ultimate soil resistance for $Z/d > 0.5$. There is no well-defined ultimate soil resistance at large deflections as recommended by API (2000).

In terms of fitting these p–y curves, many trials have been carried out to fit these curves. It was found that the experimental p–y curves could be expressed by a soil parameter that is a function of stress level. The shear wave velocity of the sand (V_s) was measured in-flight using bender elements at three depths (110, 160, and 220 mm, in model scale) in the same test package. The maximum shear modulus (G_{max}) and the maximum Young's modulus (E_{max}) were calculated using the measured (V_s) and assuming Poisson's ratio of 0.3 for dense sand. The soil pressure ($p = P/d$) can be normalized to the measured maximum Young's modulus (E_{max}).

It can be seen in Fig. 15 that after normalization all the experimental p–y curves of Z/d ratios of 1 to 3.2 collapse to a narrow band. The average fitting curve for all loading angles cases can be expressed as

$$[6] \qquad \frac{p}{E_{max}\,(Z/d)^n}\% = a\left(\frac{y}{d}\%\right)^b$$

The values of parameters n, a, and b are given in Table 2. A similar equation was recommended by Yan and Byrne (1992) assuming $n = 0$. The tests carried out by Yan and Byrne (1992) were for piles of small diameters around 0.5 m. For the current study, the pile diameter is 1.4 m. So the parameter n could be increasing by increasing the pile diameter. Figure 16 shows the variation on parameter n and $(b/a)^{0.5}$ versus tan θ. The relationships can follow the following linear functions:

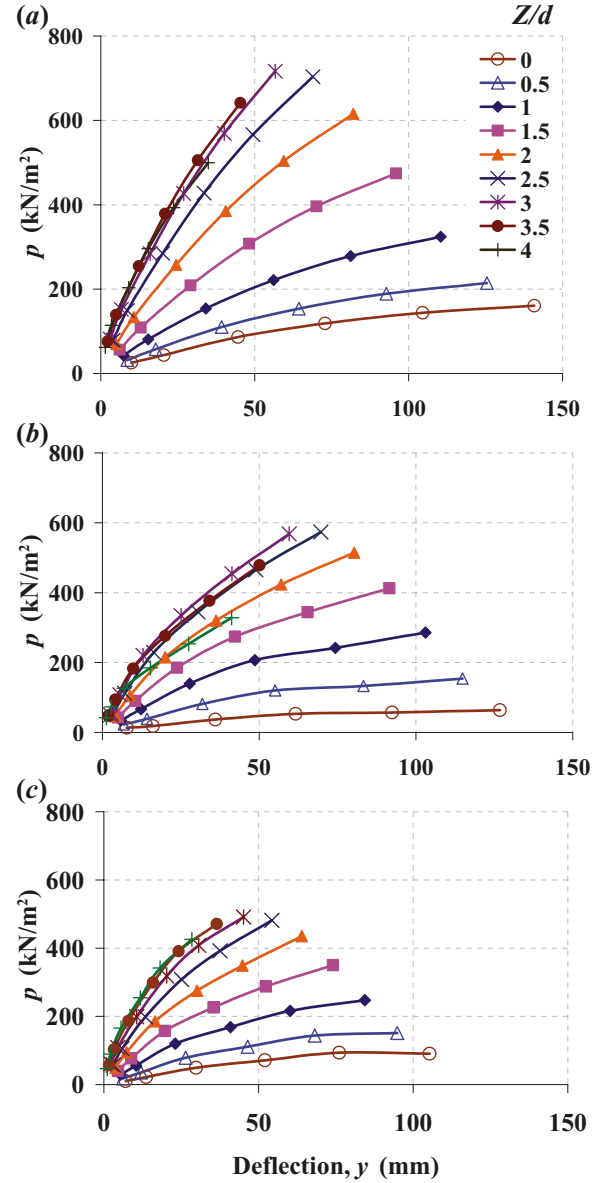**Fig. 13.** p–y curves for loading angles: (a) 0°, (b) 16°, and (c) 30°.

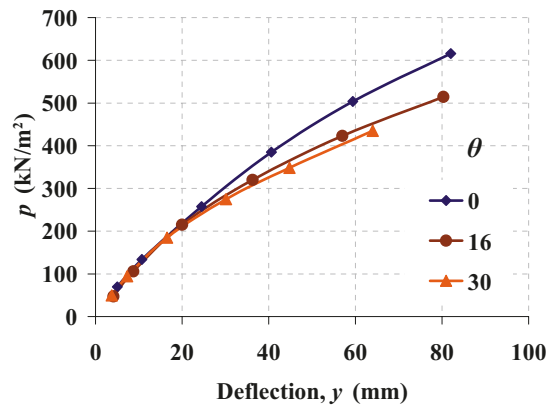**Fig. 14.** Comparison of experimental p–y curves for different loading angles – $Z/d = 2$.

Fig. 15. Normalized *p–y* curves for loading angles: 0°, 16°, and 30°.
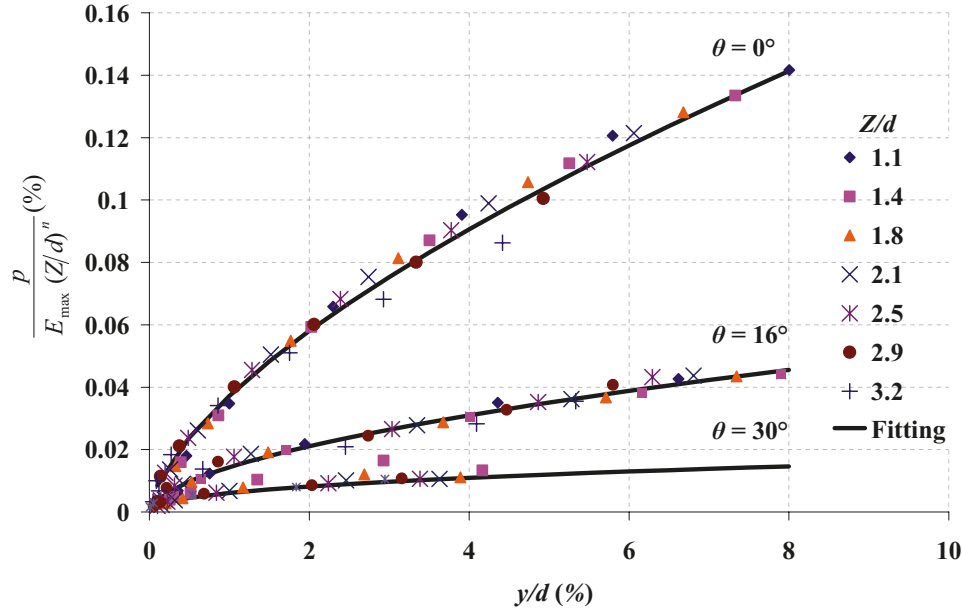
Table 2. *p–y* curve parameters.

Loading angle, θ (°)	n	a	b
0	0.5	0.037	0.64
16	1.0	0.014	0.56
30	1.5	0.006	0.42

Fig. 16. Relationship between *p–y* curve parameters and loading angle.
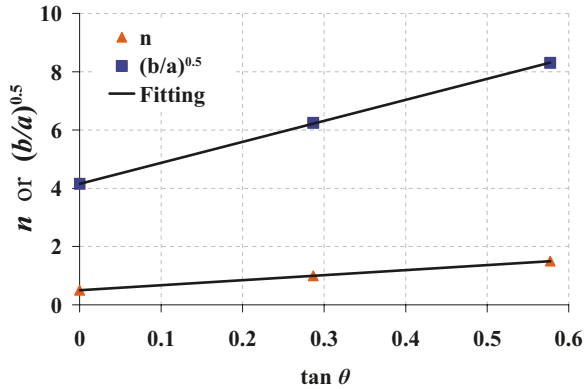
$$[7] \qquad n = 0.5 + 1.73 \tan\theta$$

$$[8] \qquad (b/a)^{0.5} = 4.15 + 7.2 \tan\theta$$

However, eqs. [7] and [8] are limited to dense sand and to the current pile flexural and axial stiffnesses. A complete design method to predict *p–y* curves for piles under inclined pullout loading cannot be provided from the present tests. Other factors (i.e., sand relative density, pile stiffness, and pile diameter) should be investigated in an experimental parametric study to see how these parameters may change with other conditions.

From these *p–y* curves, it can be seen that the curves are becoming softer as the loading changes from pure lateral to inclined pullout loading regardless of the loading angle. This means that the interaction between the lateral and vertical resistances of a pile under inclined pullout should not be neglected. A pile sub-

jected to an inclined pullout should not be designed as a pile loaded purely laterally.

Conclusion

From the present centrifuge tests results, the following conclusion can be drawn:

1. When a pile is subjected to inclined pullout loading, the tension load component will cause elastic "Poisson" radial contractions of the pile cross section, which is more significant with pipe piles as reported by Jardine et al. (2005) (ICP method).
2. This radial contraction of the pile section will cause both an increase of pile flexural stiffness and a decrease of soil confining pressure around the pile.
3. The increase of pile flexural stiffness will result in a decrease of pile bending moment. Also, the decrease of soil confining pressure will contribute to pile bending moment reduction.
4. It should be noted that this conclusion is valid for offshore driven pipe piles in dense sand where soil stresses around the pile are high, especially at the lower part of the pile due to pile driving. Both the increase in soil stresses and the tubular section of the pile will contribute to the pile section contraction when subjected to tension load.
5. The reduction of bending moment and soil pressure around the pile depends on pile axial stiffness, which controls the elastic "Poisson" radial contraction of the pile.

References

Abdel-Rahman, K., and Achmus, M. 2006. Numerical modeling of the combined axial and lateral loading of vertical piles. *In* Proceedings of the Sixth European Conference on Geotechnical Engineering, Graz, Austria.

Achmus, M., Abdel-Rahman, K., and Wörden, F. 2007. Geotechnical design of piles supporting foundation structures for offshore wind energy converters.

In Proceedings of the Seventeenth International Offshore and Polar Engineering Conference, Lisbon, Portugal.

Altaee, A., and Fellenius, B.H. 1994. Physical modeling in sand. Canadian Geotechnical Journal, **31**(3): 420–431. doi:10.1139/t94-049.

API. 2000. Recommended practice for planning. designing and constructing fixed offshore platforms-working stress design. RP2A-WSD, 21st ed. American Petroleum Institute (API).

Bhattacharya, S., Carrington, T.M., and Aldridge, T.R. 2006. Design of FPSO piles against storm loading. Offshore Technology Conference, OTC 17861.

Bouafia, A. 1999. Large lateral displacements of piles in sand – modelling in centrifuge. Geotechnical Engineering for Transportation Infrastructure, Barends et. al., Balkema, Rotterdam.

Broms, B.B. 1965. Piles in cohesionless soil subject to oblique pull. Discussion. Journal of the Soil Mechanics and Foundations Division, ASCE, **91**(4): 199–205.

Chakrabortty, P. 2008. Seismic liquefaction of heterogeneous soil: mechanism and effects on structural response. Ph.D. thesis, Memorial University of Newfoundland, N.L.

Chattopadhyay, B.C., and Pise, P.J. 1986. Ultimate resistance of vertical piles to oblique pulling load. *In* Structural Engineering and Construction: Advances and Practice in East Asia and The Pacific, Proceedings of The First East Asian Conference on Structural Engineering and Construction, Bangkok, Thailand. Vol. 1, pp. 1632–1641.

Das, B.M., Seeley, G.R., and Raghu, D. 1976. Uplift capacity of model piles under oblique loads. Journal of the Geotechnical Engineering Division, ASCE, **102**(9): 1009–1013.

De Nicola, A., and Randolph, M.F. 1997. The plugging behaviour of driven and jacked piles in sand. Géotechnique, **47**(4): 841–856. doi:10.1680/geot.1997.47.4.841.

De Nicola, A., and Randolph, M.F. 1999. Centrifuge modelling of pipe piles in sand under axial loads. Géotechnique, **49**(3): 295–318. doi:10.1680/geot.1999.49.3.295.

Dief, H.M. 2000. Evaluating the liquefaction potential of soils by the energy method in the centrifuge. Ph.D. thesis, Case Western Reserve University.

Dyson, G.J., and Randolph, M.F. 2001. Monotonic lateral loading of piles in calcareous sand. Journal of Geotechnical and Geoenvironmental Engineering, ASCE, **127**(4): 346–352. doi:10.1061/(ASCE)1090-0241(2001)127:4(346).

Hesar, M. 1991. Behaviour of pile-anchors subjected to monotonic and cyclic loading, Ph.D. thesis, University of Sunderland, UK.

Ismael, N.F. 1989. Field tests on bored piles subject to axial and oblique pull. Journal of Geotechnical Engineering, **115**(11): 1588–1598. doi:10.1061/(ASCE)0733-9410(1989)115:11(1588).

Jamnejad, G.H., and Hesar, M.H. 1995. Stability of pile anchors in the offshore environment. Transactions of the Institue of Marine Engineers, **107**: 119–134.

Jardine, R.J., Chow, F.C., Overy, R.F., and Standing, J.R. 2005. ICP design methods for driven piles in sands and clays. Thomas Telford, London.

Leshukov, M.R. 1975. Effect of oblique extracting forces on single piles. Soil Mechanics and Foundation Engineering, **12**(5): 300–301. (English translation of Osnovaniya, Fundamenty i Mekhanika Gruntov.) doi:10.1007/BF01706173.

Mezazigh, S., and Levacher, D. 1998. Laterally loaded piles in sand: slope effect on *P-Y* reaction curves. Canadian Geotechnical Journal, **35**(3): 433–441. doi:10.1139/t98-016.

Nunez, I.L., Hoadley, P.J., Randolph, M.F., and Huetett, J.M. 1988. Driving and tension loading of piles in sand on centrifuge. *In* Proceedings of Centrifuge' 88, Paris, France. pp. 352–362.

Ovesen, N.K. 1979. The scaling law relationship. *In* Proceedings of 7th European Conference on Mechanics and Foundation Engineering, Brighton. Vol. 4, pp. 319–323.

Poulos, H.G., and Davis, E.H. 1980. Pile foundation analysis and design. John Wiley & Sons, New York.

Ramadan, M.I., Butt, S.D., and Popescu, R. 2009*a*. Pipe piles under mooring forces. *In* Proceedings of the 17th International Conference of Soil Mechanics and Geotechnical Engineering, ICSMGE'09, Alexandria, Egypt, 5–9 October.

Ramadan, M.I., Butt, S.D., and Popescu, R. 2009*b*. Finite element modeling of offshore anchor piles under mooring forces. *In* Proceedings of the 62nd Canadian Geotechnical Society Conference, GeoHalifax'09, Halifax, N.S.

Remaud, D. 1999. Pieux sous charges latérales: Étude expérimentale de l'effet de groupe. These de Doctorat, Université de Nantes.

Wijewickreme, D., Sriskandakumar, S., and Byrne, P. 2005. Cyclic loading response of loose air-pluviated Fraser River sand for validation of numerical models simulating centrifuge tests. Canadian Geotechnical Journal, **42**(2): 550–561. doi:10.1139/t04-119.

Yan, L., and Byrne, P.M. 1992. Lateral pile response to monotonic head loading. Canadian Geotechnical Journal, **29**(6): 955–970. doi:10.1139/t92-106.

Yoshimi, Y. 1964. Piles in cohesionless soil subjected to oblique pull. Journal of the Soil Mechanics and Foundations Division, ASCE, **90**(6): 11–24.